Nano Research
2022, 15(10): 9531–9543

ISSN 1998-0124 CN 11-5974/O4
https://doi.org/10.1007/s12274-022-4883-6

Research Article

Multi-hierarchical flexible composites towards superior fire safety and electromagnetic interference shielding

Kexin Chen[1], Miao Liu[1], Yongqian Shi[1] (✉), Hengrui Wang[1], Libi Fu[2], Yuezhan Feng[3], and Pingan Song[4]

[1] College of Environment and Safety Engineering, Fuzhou University, Fuzhou 350116, China
[2] College of Civil Engineering, Fuzhou University, Fuzhou 350116, China
[3] Key Laboratory of Materials Processing and Mold Ministry of Education, National Engineering Research Center for Advanced Polymer Processing Technology, Zhengzhou University, Zhengzhou 450002, China
[4] Centre for Future Materials, University of Southern Queensland, Springfield, QLD 4350, Australia

Received: 9 July 2022 / **Revised:** 5 August 2022 / **Accepted:** 8 August 2022

ABSTRACT

Vast amounts of electromagnetic waves are generated in modern society, which severely endanger human health and cause instrument disturbance. Furthermore, practical application of electromagnetic shielding polymer-based materials aspires to flame retardancy. Herein, cellulose acetate butyrate modified ammonium polyphosphate (CAPP) and phosphoramide flame retardant decorated short carbon fiber (MSCF) were synthesized separately and then simultaneously blended into thermoplastic polyurethane (TPU) to prepare a series of flame retardant TPU composites. Then, the multi-hierarchical flexible TPU/CAPP/MSCF composites were fabricated via our self-developed air-assisted thermocompression method. The results revealed that the TPU/CAPP/MSCF showed improved thermal stability. Moreover, the TPU/10CA/2.5F incorporated with 10.0 wt.% CAPP and 2.5 wt.% MSCF respectively exhibited 77.8% and 58.6% reduction in peak of heat release rate (PHRR) and total heat release (THR), compared to those of pure TPU. In addition, the TPU/10CA/2.5F passed the UL-94 V-0 rating test and achieved a higher limit oxygen index (LOI) (27.3%) than pure TPU (21.7%). In the case of electromagnetic interference shielding effectiveness (EMI SE), the TPU/10CA/10.0F-SW with 10 wt.% CAPP and 10 wt.% MSCF dispersed in the surface layer and $Ti_3C_2T_x$ MXene intercalated in the interlayer exhibited EMI SE of 43.8 dB in X band and 32.0 dB in K band. Summarily, synergistic effect between CAPP and MSCF together with scattered and multiply adsorbed effect of MSCF, MXene and CAPP was responsible for fire safety and EMI shielding property improvements. This work provides a fascinating strategy for fabricating multi-hierarchical flexible TPU composites with outstanding flame retardant and EMI shielding performances.

KEYWORDS

MXene, multi-hierarchical structure, flame retardancy, electromagnetic interference shielding, air-assisted thermocompression

1 Instructions

In recent years, the soaring popularity of portable electronic devices contributes to considerable electromagnetic pollution [1–3]. Electromagnetic interference (EMI) not only deteriorates precision equipment and apparatus, but also causes harm to human health [4, 5]. The design of novel materials or composites for effectively shield against EMI has become a front-burner issue. Compared to metal materials, polymer based electromagnetic shielding materials with lightness, chemical stability, good processability, and high efficiency show broad application prospects. As one of the versatile engineering materials, thermoplastic polyurethane (TPU) shows excellent physical and chemical properties, which is suitable as a precursor of functioned electromagnetic shielding materials. Unfortunately, the widespread application of polymers, including TPU materials, is limited due to their electrical insulation and flammability. Therefore, it is urgent to develop functioned TPU composites integrated with flame retardant and electromagnetic shielding properties.

It is well known that the combination of flame retardant materials and conductive fillers in the polymers can simultaneously improve its flame retardant and electromagnetic shielding performances [1]. Regarding the flame retardancy of TPU, halogen-free flame retardants containing nitrogen-, silicon-, phosphorus-, and some nano additives have a widespread application [6–9]. Especially, modified ammonium polyphosphate (APP) has emerged as a typical environmentally friendly intumescent flame retardant which can effectively improve the flame retardant properties of the polymers while enhancing its mediocre compatibility with polymer interfaces [10, 11]. Appropriate surface modifiers can better enhance the interaction between APP and polymer matrix. Cellulose esters are bio-based materials with low toxicity and high stability [12]. Cellulose acetate butyrate (CAB) combines the advantages of acetic acid and butyric acid, where acetic acid has good flame retardancy while butyric acid possesses better matrix-filler compatibility [13]. Therefore, CAB is very suitable as a shell material for microcapsules.

Carbon-based conductive fillers are favored by researchers because of their light weight, corrosion resistance, and tunable

Address correspondence to shiyq1986@fzu.edu.cn

properties [14–16]. Particularly, carbon-based conductive fillers can be divided into three categories according to the degree to which their spatial dimensions are constrained by the nanoscale, that is, zero-dimensional materials (carbon black [17]), one-dimensional materials (carbon nanotube [18] and carbon fiber [19]), and two-dimensional materials (exfoliated MXene [20], graphene [21, 22], and reduced graphene [23]). Specifically, short carbon fiber (SCF) shows a characteristic of lightweight, large aspect ratio, and chemical stability, which is an optimal candidate for application in electromagnetic shielding products [19, 24, 25]. Moreover, there is no contradiction between modification of conductive fillers and formation of conductive networks. For instance, Lin et al. fabricated silver-nanoparticle-decorated functional reduced graphene oxide (Ag@FRGO) and demonstrated that the homogeneous dispersion of the as-prepared additive promoted the formation of conductive networks in the polymer matrix [26]. It is found that the functionalized conductive fillers can be equipped with adjustable multifunctional attributes.

It is worth noting that the electromagnetic shielding properties of composites are closely related to not only the type and content of the fillers but also the composition structure. Various attempts have been implemented to explore the reasonable structural design. Li et al. reported a rigid carbon foam through carbonization of thermosetting polyimide foam [27]. The results indicated that the sample CF-1200 (carbonized at 1,200 °C) showed superior EMI shielding effectiveness (EMI SE) (> 50 dB). Ji et al. fabricated a TPU-based electromagnetic shielding material via coextrusion technology, and maximum EMI SE of 38.5 dB was obtained with less than 4 wt.% carbon nanotubes (CNTs) [28]. In general, the structure of electromagnetic shielding materials can be classified into three categories, namely porous structure [29, 30], segregated structure [31], and layered structure [32, 33]. However, the microlayer co-extrusion method is highly dependent on the molding equipment. In addition, porous polymers are easy to leak electromagnetic waves, while segregated polymers have a greater influence on the loss of mechanical properties. In contrast, the layered sandwich structure is relatively easy to be constructed, and the hierarchy order can be adjusted and controlled to meet diverse requirements [34]. The choice of the interlayer of the layered sandwich structure is worth considering. As a new type of two-dimensional sheet material, titanium carbide (MXene, $Ti_3C_2T_x$) can be used for dual applications in the fields of flame retardancy and electromagnetic shielding [35–39]. In addition, the intercalation ability of TPU makes it easy to filter into membranes. Therefore, MXene film is a good choose as a conductive intermediate layer.

In this work, the SCFs were modified by phosphoramide flame retardant to obtain functionalized modified SCF (MSCF). APP was microencapsulated by CAB to prepare the CAPP. Then, MSCF and CAPP were melt-blended and hot pressed into TPU matrix to obtain flame retardant TPU composites plates, which could act as surface layer of the multi-hierarchical flexible TPU composites. Considering the fact that $Ti_3C_2T_x$ film is very sensitive to moist-air, the TPU modified $Ti_3C_2T_x$ film was used as middle layer. Notably, the structure of TPU composites/modified $Ti_3C_2T_x$ film/TPU composites was assembled by our developed air assisted thermocompression technology. The thermal, flame retardant, and electromagnetic shielding properties of multi-hierarchical flexible TPU composites were investigated in depth. Finally, the possible flame retardant- and electromagnetic shielding-mechanisms were discussed.

2 Experimental section

2.1 Raw materials

Thermoplastic polyurethane elastomer (TPU, 65E85) was supplied by Bangtai Chemical Industry Co., Ltd. (Baoding, China). Ti_3AlC_2 powders (400 mesh, 99%) was obtained from the 11 Technology Co., Ltd. (Changchun, China). Lithium fluoride (LiF, 98.5%), concentrated hydrochloric acid (HCl, 36%–38%), and anhydrous ethanol (AR) were all purchased from the Sinopharm Chemical Reagent Co., Ltd. (Shanghai, China). APP ($n \geq 1{,}000$) was afforded by Shanghai Aladdin Biochemical Technology Co., Ltd. (Shanghai, China). Alkylphenol ethoxylates (emulsifier OP-10, AR) was provided by Tianjin Kemiou Chemical Reagent Co., Ltd. (Tianjin, China). CAB (35%–39%) and 2,4-toluene diisocyanate (TDI, 98%) were obtained from Shanghai En Chemical Technology Co., Ltd. (Shanghai, China). SCF (95% carbon content) was produced in Dongli Carbon Fiber Co., Ltd. (Guangdong, China). 4,4'-Diaiminodiphenyl ether (DDE, AR, ≥ 99.0%), phosphorus oxide trichloride ($POCl_3$, AR), ethyl acetate (AR, ≥ 99.5%), triethylamine (AR, ≥ 99.0%), acetonitrile (AR, ≥ 99.0%), and N,N-dimethylformamide (DMF, AR, ≥ 99.0%) were all provided by Sinopharm Chemical Reagent Co., Ltd. (Shanghai, China). Nitric acid (HNO_3, 65%–68%, AR) and calcium chloride anhydrous ($CaCl_2$, AR) were supported by Xilong Scientific Co., Ltd. (Guangdong, China).

2.2 Preparation of MXene films

According to our previous work, the dispersion of $Ti_3C_2T_x$ MXene was prepared by etching Ti_3AlC_2 using LiF and HCl [40, 41]. Afterwards, a certain amount of MXene suspension was dewatered by vacuum filtration to prepare MXene film, and thickness of the MXene film was controlled to be around 24.48 ± 1.19 μm. Especially, the obtained MXene film was wrapped with TPU sol which was dissolved in DMF solution (Fig. 1(a)). After drying, the weight gain of the impregnated MXene was 28.03 wt.%.

2.3 Synthesis of CAB modified APP

The CAPP was prepared according to Ref. [13]. A three-necked flask was equipped with a stirrer and a condenser coupled with a drying tube containing $CaCl_2$. Firstly, 4.00 g of CAB and 150 mL of ethyl acetate were added into a 500 mL three-necked flask under mechanical stirring until the temperature reached 80 °C. When the CAB was completely dissolved, 60.00 g APP and 0.60 g OP-10 were added into the suspension. After stirring for 15 min, 4.00 g of TDI was introduced dropwise within 30 min. Then, the reaction was maintained for 6 h. Finally, the product was cooled to room temperature and washed with ethyl acetate and deionized water by centrifugation. The collected white precipitate was named CAPP.

2.4 Preparation of phosphoramide flame retardant modified SCF

In the preparatory stage, SCF was ultrasonically dispersed in absolute ethanol for 0.5 h. The processed SCF was oxidized in concentrated HNO_3 at 100 °C for 2 h, and then washed several times with deionized water until pH = 6. In a typical process, 5.00 g of SCF and 500 mL of acetonitrile solvent were mixed and ultrasonically dispersed for 30 min. Under the conditions of ice bath and nitrogen, 33.30 g of triethylamine and 9.90 g of DDE were added to the above solution. Afterwards, the mixture of 200 mL of acetonitrile and 5.00 g of $POCl_3$ was further thrown to the mixed solution at a speed of 4–5 s/drop. After reacting in ice bath for 1 h, the mixture was gradually heated to 50 °C in oil bath and refluxed for 24 h. Finally, the product (MSCF) was filtered, washed with acetonitrile and deionized water, and then dried under vacuum at 50 °C.

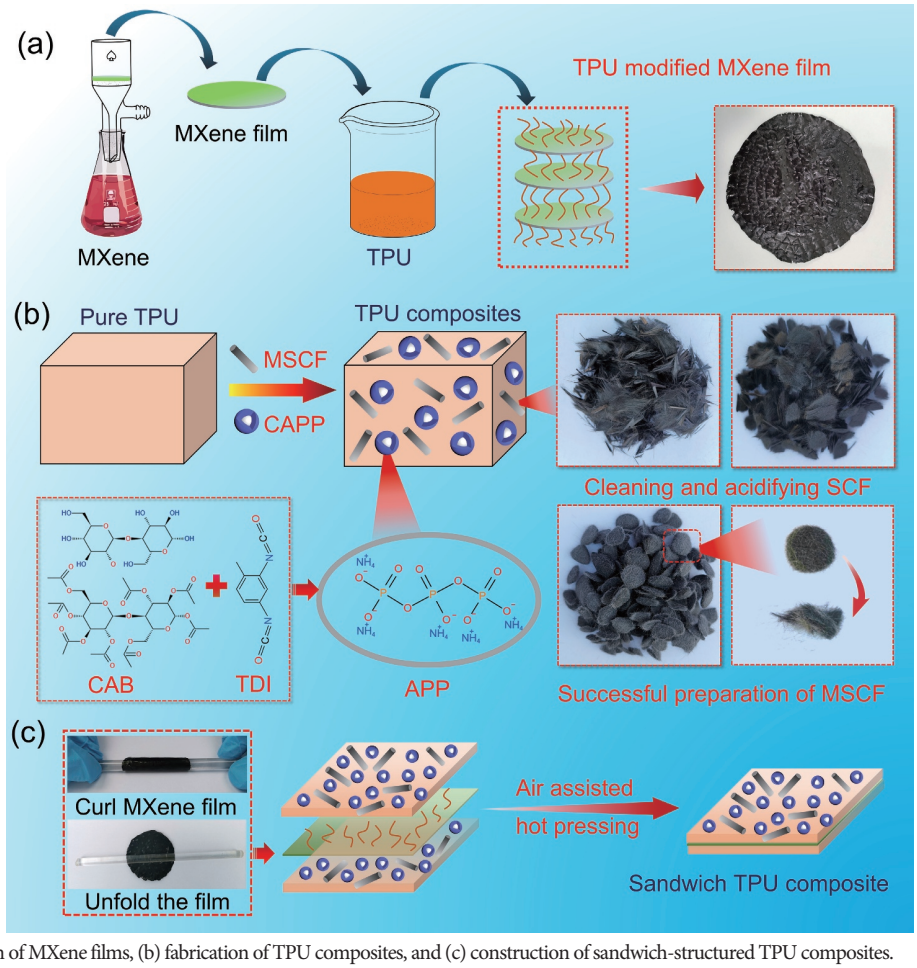

Figure 1 (a) Preparation of MXene films, (b) fabrication of TPU composites, and (c) construction of sandwich-structured TPU composites.

2.5 Fabrication of TPU composites

TPU composite grains were obtained by melt blending with a certain proportion of SCF and CAPP at 180 °C in a SU-70 twin roller mill (Suyan Science & Technology Co., Ltd., Changzhou, China). Subsequently, the TPU grains were hot pressed at 190 °C under a pressure of 10 MPa to obtain TPU composite plates. For example, the TPU composite containing 10 wt.% CAPP and 2.5 wt.% MSCF was labelled as TPU/10CA/2.5F (where CA and F meant CAPP and MSCF, respectively) (Fig. 1(b)). In particular, TPU composite plates with a thickness of 0.50 mm were used to fabricate multi-hierarchical flexible TPU composites, while the TPU composite plates with a thickness of 1.00 mm were prepared for comparison. The detailed information of the TPU composites is exhibited in Table 1.

2.6 Construction of multi-hierarchical flexible TPU composites

According to the above operation, TPU composites with the thickness of 0.5 mm were prepared. It is noted that the novel air-assisted hot-pressing method instead of the traditional hot-pressing method was implemented to construct multi-hierarchical flexible TPU composites. Based on the principle of heat absorption and heat dissipation, a typical preparation process was described as follows. In a typical process, single-layered TPU/10CA/5.0F plate (0.5 mm of the thickness) was softened and hot-pressed with a TPU wrapped $Ti_3C_2T_x$ film. Then, another identical TPU/10CA/5.0F plate was softened and hot-pressed in combination with the aforementioned samples. The multi-hierarchical flexible TPU composite was denoted as TPU/10CA/5.0F-SW (Fig. 1(c)).

2.7 Characterization and measurements

Morphology observation of the fracture surfaces of TPU samples was obtained by field scanning electron microscopy (SEM, FEI Nova NanoSEM 230, USA). Morphologies of flame retardant additives and char residues of TPU composites were observed by ultra-high resolution field emission scanning electron microscopy (FESEM, Verios G4, USA) coupled with energy dispersive X-ray (EDX, Octane Elect Super, EDAX Inc Company). The samples were sprayed with a thin layer of gold cladding before observation. Transmission electron microscopy (TEM) image was investigated by a JEM-2100 instrument with an accelerating voltage of 200 kV (JEOL Co., Japan). The thickness of exfoliated $Ti_3C_2T_x$ nanosheet was evaluated by an atomic force microscopy (AFM, Veeco DI Multimode V, USA) in scanning probe mode. Fourier transform infrared (FTIR) spectra were conducted using a Nicolet iS50 spectrophotometer (Thermo Fisher Instrument Co., USA) in the scanning range from 400 to 4,000 cm^{-1}. X-ray diffraction (XRD) patterns were acquired using a DY1602/Empyrean X-ray diffractometer (Panalytical, Netherlands) equipped with Cu Kα radiation (λ = 1.54178 Å). The surface composition of oxidized SCF (SCF-O) and MSCF was conducted by an ESCALAB 250 X-ray photoelectron spectroscopy (XPS, VG Co., USA) equipped with Al/Mg dual anode target and 0.6 eV of energy resolution. Water contact angle (WCA) test was recorded using CAM2008 software at room temperature. Thermogravimetric analysis (TGA) was implemented on a Q5000 thermal analyzer (TA Co., USA) from room temperature to 800 °C at a heating rate of 20 °C/min under N_2 atmosphere. Fire hazard assessment was conducted on a TTech-GBT16172-2 cone calorimetry (TESTech, Suzhou, China) under a flux of 35 kW/m^2 according to ISO 5660. The limit oxygen index (LOI) values were obtained by a LOI device (Model

Table 1 Detailed information of sandwich structured TPU composites

Sample no.	TPU (wt.%)	CAPP (wt.%)	MSCF (wt.%)	Inserting $Ti_3C_2T_x$ film
TPU	100.00	0.00	0.00	No
TPU/12.5CA	87.50	12.50	0.00	No
TPU/10CA/2.5F	87.50	10.00	2.50	No
TPU/10CA/5.0F	85.00	10.00	5.00	No
TPU/10CA/10.0F	80.00	10.00	10.00	No
TPU-SW	100.00	0.00	0.00	Yes
TPU/12.5CA-SW	87.50	12.50	0.00	Yes
TPU/10CA/2.5F-SW	87.50	10.00	2.50	Yes
TPU/10CA/5.0F-SW	85.00	10.00	5.00	Yes
TPU/10CA/10.0F-SW	80.00	10.00	10.00	Yes

HC-2, Jiangning Analytical Instrument Co., Ltd., Nanjing, China) according to the ASTM D2863-2010 with a specimen dimension of 100 mm × 6.7 mm × 3 mm. The vertical burn test (UL-94) was measured using a horizontal and vertical burning tester (model CZF-II, Jiangning Analytical Instrument Co., Ltd., Nanjing, China) according to the ASTM D3801-2010 with dimensions of 127 mm × 13 mm × 10 mm. Laser Raman spectra (LRS) were acquired using a Renishaw Invia Raman microscope (Invia Reflex, Renishaw Invia, UK) with a 532 nm argon ion laser at a spectroscopic resolution of 1.2 cm^{-1}. Anti-electromagnetic interference ability of TPU samples in frequency range of 8.2–12.4 GHz (X-band) and 18.2–26.5 GHz (K-band) was recorded with a N5222B vector network analyzer (Keysight Technologies, USA). All the samples were cut into a rectangle with the dimension of 25.6 mm × 11.2 mm. The key parameters including reflection coefficient (R), absorption coefficient (A), and transmission coefficient (T) were calculated by Eqs. (1)–(3) [42]

$$R = |S_{11}|^2 \quad (1)$$

$$T = |S_{21}|^2 \quad (2)$$

$$A = 1 - R - T \quad (3)$$

Since the thickness of the multilayered composites was failure to exceed the skin depth, multiple internal reflection could be ignored. According to the theoretical model of shielded transmission line, the SE_T, SE of A (SE_A), and SE of R (SE_R) of all TPU multilayered composites were expressed as Eqs. (4)–(6) [42]

$$SE_R = 10\lg(1-R) = 10\lg(1-|S_{11}|^2) \quad (4)$$

$$SE_A = -10\lg(T/1-R) = 10\lg(|S_{21}|^2/1-|S_{11}|^2) \quad (5)$$

$$SE_T = SE_R + SE_A \quad (6)$$

where S_{11} and S_{21} presented scattering parameters.

3 Results and discussion

3.1 Morphology and thermal stability of flame retardants

The morphologies of the additives were characterized by SEM, TEM, and AFM. Figure 2(a) shows the stacked layered structure of Ti_3AlC_2. After the elimination of aluminum element, $Ti_3C_2T_x$ exhibits distinct lamellar structure with alternating void layers (Fig. 2(b)). Compared with $Ti_3C_2T_x$ powder, the layered structure of $Ti_3C_2T_x$ film is more obvious and regular (Fig. 2(c)). The microstructure and thickness of the exfoliated $Ti_3C_2T_x$ monolayers are obtained by TEM and AFM (Figs. 2(d)–2(f)). $Ti_3C_2T_x$ displays ultrathin flake morphology with a thickness of 2.31 ± 0.01 nm. The measured thickness is larger than that in Ref. [35], resulting from the interlayer water between the $Ti_3C_2T_x$ sheets. APP shows block-like structure with smooth surface while the surface of CAPP becomes rough. Moreover, as-synthesized CAPP (126.1°) exhibits a much larger water contact angle than APP (14.3°), demonstrating the successful encapsulation of APP by CAB. By comparing Figs. 2(i) and 2(j), the chemical transition of SCF-O to MSCF can be clearly visible. The surface of SCF-O has a rough texture, whereas the surface of the modified MSCF is loaded with granular beads, demonstrating successful loading of phosphoramide-based flame retardants. As shown in Figs. 2(k) and 2(l), element composition of MSCF is C, O, N, and P, which is reasonable to speculate the successful crosslinking between modifier and SCF.

XRD patterns of Ti_3AlC_2, $Ti_3C_2T_x$, APP, and CAPP are displayed in Fig. S1(a) in the Electronic Supplementary Material (ESM). The characteristic peak occurs at 38.7° corresponding to (104) crystal plane for Ti_3AlC_2 [43, 44]. Upon the etching, the (104) diffraction peak disappears, and the (002) diffraction peak shifts from 9.5° to 7.7°, which indicates the successful etching of $Ti_3C_2T_x$. In terms of APP and CAPP, the diffraction peaks of modified APP are similar to those of the original APP, while the corresponding peak intensity totally decreases. FTIR instruments were conducted to further analyze microscopic chemical structure of flame retardants. Similar to the previous report [13], the typical band of APP at 3,206, 1,258, 1,076, 1,012, 883, and 799 cm^{-1} are assigned to N–H bond, P–O bond, P–O symmetric stretching vibration, symmetric vibration of PO_2 and PO_3, P–O asymmetric stretching vibration, and P–O–P bond, respectively (Fig. S1(b) in the ESM). The absorption bands of CAPP are also similar to those of APP. Specially, the absorption band at 1,750 cm^{-1} (C=O stretching) is ascribed to cross-linking of CAB. In the case of MSCF (Fig. S1(c) in the ESM), the absorption bands at 3,444, 1,635, and 1,506 cm^{-1} are ascribed to the hydroxyl group and aromatic compounds [45]. After grafting phosphoramide flame retardant onto the surface of SCF-O, there are several new absorption bands appear in MSCF. These absorption bands include 1,506 (P=O stretching), 1,381 (C–N stretching), 1,211 (C–O stretching), 926, and 873 cm^{-1} (P–N stretching) [46, 47]. Aforementioned vibrational features reveal that the structural units of $POCl_3$ and DDE can be successfully grafted onto SCF-O by polycondensation reaction.

To reveal more surface information, high-resolution XPS was used to detect chemical constitution of SCF-O and MSCF. The wide-scanning spectra and high-resolution spectra are portrayed

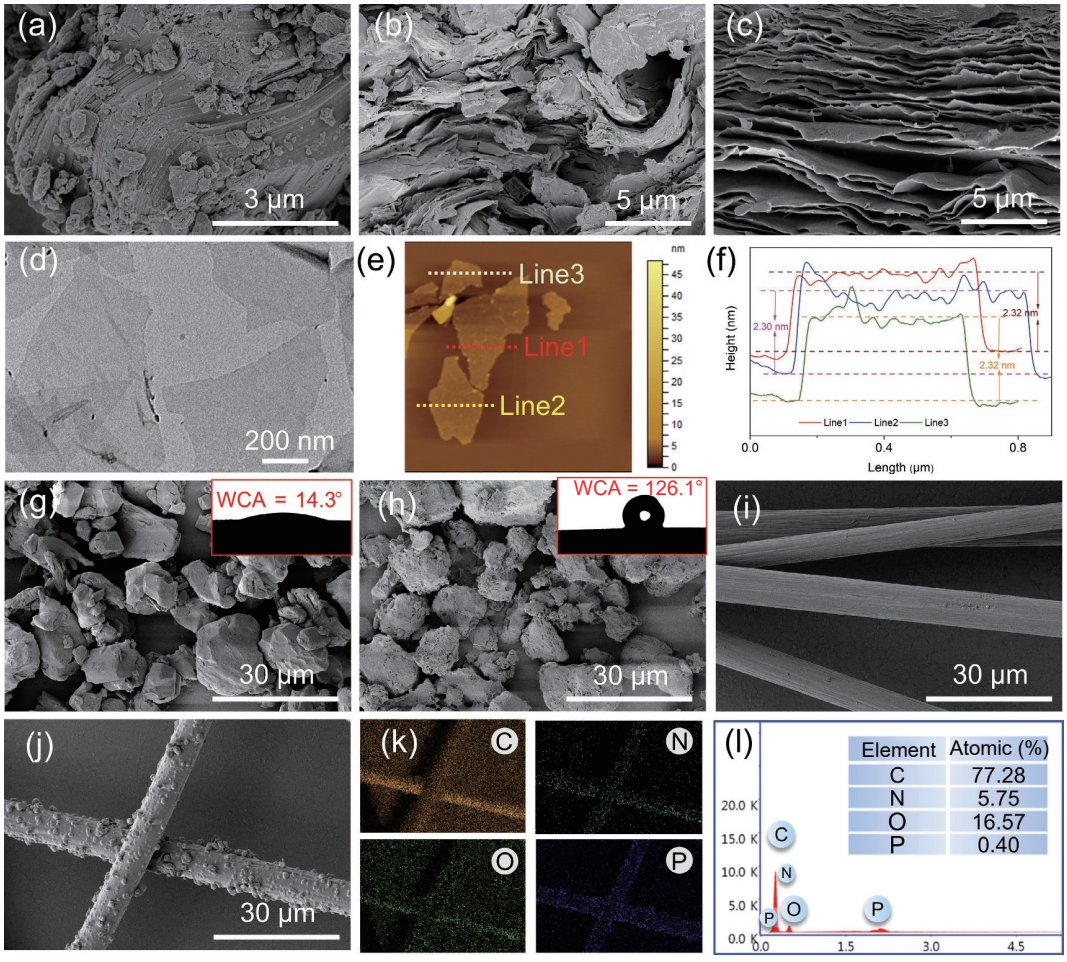

Figure 2 SEM images of (a) Ti_3AlC_2, (b) $Ti_3C_2T_x$ power, (c) $Ti_3C_2T_x$ film, (g) APP, (h) CAPP, (i) SCF-O, and (j) MSCF. (d) TEM image of $Ti_3C_2T_x$ nanosheet. (e) AFM image of $Ti_3C_2T_x$ nanosheet. (f) The corresponding thickness curves of (e). (k) Elemental mapping images of (j). (l) Elemental content analysis of (j).

in Figs. S1(d)–1(f) in the ESM. The XPS survey spectra show that SCF-O is mainly composed of C, N, and O elements (Fig. S1(d) in the ESM). In contrast, MSCF presents higher intensities of C and N elements and lower intensity of O element than SCF-O. Moreover, new signals of Cl and P elements can be observed in MSCF, which is mainly due to the introduction of $POCl_3$. However, the Cl element originates from the incomplete filtration of MSCF, which is unstable and cannot be polymerized to the segment of the modifier. High-resolution XPS spectra of N 1s and O 1s core levels of SCF-O and MSCF are also analyzed. The deconvolution of N 1s peak for both SCF-O and MSCF shows two individual component peaks (Fig. S1(e) in the ESM). For SCF-O, the N components located at 400.3 and 405.5 eV correspond to C–N=C and $–NO_2$, respectively. The peak of C–N=C originates from the carbonization process of SCF [48] while the $–NO_2$ component peak is derived from oxidation of SCF by HNO_3 [49]. In the XPS spectrum of MSCF, binding energies occurring at 399.0 and 401.5 eV are assigned to pyridine-N-oxides and pyrrolic, respectively upon the combination of DDE [50]. In the O 1s spectrum (Fig. S1(f) in the ESM), the environment of SCF-O can be distinguished into three peaks located at 531.3, 532.6, and 533.3 eV, which are attributed to C=O/O=C–OH, C–O–C/C–OH, and O_2/H_2O, respectively [51]. After the surface is grafted with phosphoramide flame retardant, MSCF can be deconvolved into two new peaks appearing at 530.8 and 533.0 eV, which are assigned to C=O/O=C–OH and P=O, respectively [52]. These phenomena can further confirm the successful crosslinking of phosphoramide flame retardant onto the surface of SCF. The schematic diagram for the preparation procedure of functionalized SCF is illustrated in Fig. S1(g) in the ESM.

Thermogravimetric analysis was used to compare the thermal stability of the additives (Fig. S1(h) in the ESM). $Ti_3C_2T_x$ and SCF have strong heat resistance at 700 °C and still retain residues of 96.20 wt.% and 98.71 wt.%, respectively. However, residual content of MSCF is decreased, due to the reason that the cross-linked network containing unstable elements on the surface can be early degraded. Similarly, CAPP (41.27 wt.%) has less residue than APP (49.37 wt.%) at 700 °C.

3.2 Morphological analysis of TPU and its multi-hierarchical flexible composites

After brittle fracture with liquid nitrogen, the interfacial compatibility between the TPU matrix and fillers, and the morphology of the multi-hierarchical structure can be observed by SEM. Morphologies of the multi-hierarchical flexible TPU composites are plotted in Figs. 3(a)–3(e). It is found that TPU sheets are successfully attached to the MXene film in all the samples. However, due to the external force during the sample preparation, a slight gap appears between the TPU and MXene films. To better analyze the microstructure of all the multi-hierarchical flexible samples, morphologies of TPU composites were further dissected. Figures 3(f)–3(j) display the surface morphologies of a series of TPU composites. Pure TPU shows smooth surface with wavy creases (Fig. 3(f)). With the addition of 12.5 wt.% CAPP, fine particles appear on the surface of the TPU/12.5CA without agglomeration, which indicates the good dispersion of CAPP in the TPU matrix (Fig. 3(g)). As the content of SCF varies from 2.5 wt.% to 10.0 wt.% for TPU/12.5CA/F-SW, the surface of the TPU composite also appears a growing cylindrical substance (Figs. 3(h)–3(j)). All additives are well

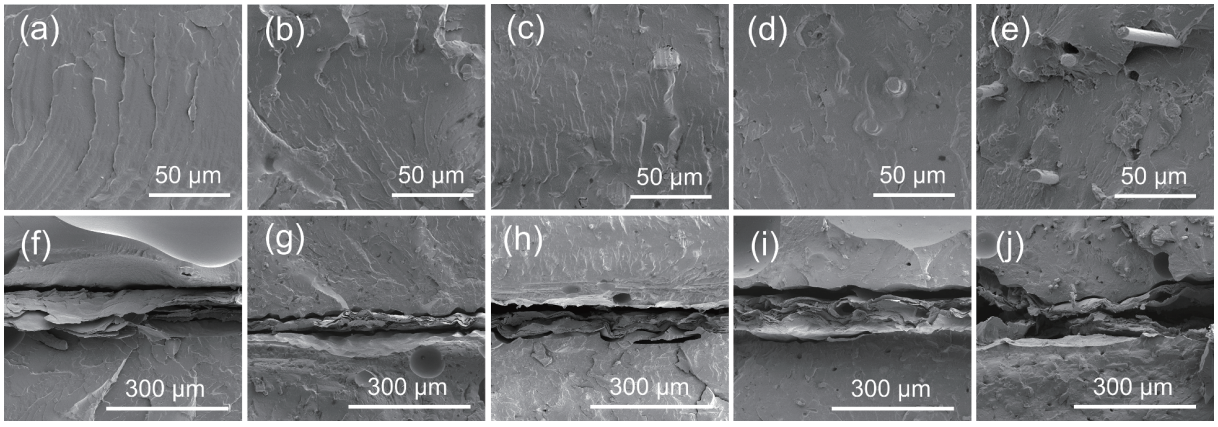

Figure 3 SEM images of freeze-fractured surface of ((a) and (f)) TPU-SW, ((b) and (g)) TPU/12.5CA-SW, ((c) and (h)) TPU/10CA/2.5F-SW, ((d) and (i)) TPU/10CA/5.0F-SW, and ((e) and (j)) TPU/10CA/10.0F-SW.

encapsulated in the TPU host without any voids and agglomerations, indicative of the excellent interfacial interactions between TPU matrix and additives.

3.3 Thermal properties of TPU/CAPP/MSCF composites

The degradation behavior of TPU composites under nitrogen condition was assessed by TGA, and the related results are shown in Fig. 4 and Table S1 in the ESM. Our previous research have confirmed that $Ti_3C_2T_x$ films are non-flammable and high thermal stability [53]. Therefore, thermal and combustion performances are considered for TPU composites without a sandwich structure. In order to verify the synergistic effect between CAPP and MSCF, the comparison between the experimental and theoretical values was conducted. It can be observed from Figs. 4(a) and 4(c) that all TPU and its composites undergo two stages of degradation, where the first stage is ascribed to the decomposition of hard segment in TPU, and the second stage is caused by further dissociation of polyhydric alcohols in soft segment [35]. Pure TPU shows the initial decomposition temperature (T_{-5}) of 313.3 °C and only 1.20 wt.% residue left at 700 °C. Upon the introduction of CAPP, the TPU/12.5CA exhibits a lower T_{-5}. After combination of CAPP and MSCF, the T_{-5} values of TPU composites are even lower. This can be explained by the earlier decomposition of the TPU segment induced by phosphorus-containing component [54, 55]. Similarly, the temperatures at 50% weight loss rate (T_{-50}), maximum weight loss rate (T_{max1} and T_{max2}) are also decreased variedly. It is noted that the residual char of TPU/12.5CA is higher than that of pure TPU, suggesting that the CAPP can effectively promote the charring of TPU matrix. With the addition of MSCF, the content of char residue for TPU/CAPP/MSCF composites increases significantly. For example, TPU/10CA/10.0F shows 31.86 wt.% of char residues, which is 26.55 times higher than that of pure TPU. These results reveal that CAPP and MSCF have a huge synergistic effect on the catalytic charring of TPU.

To highlight the effect of interaction of CAPP and MSCF on thermal property of TPU composites, experimental and calculated TGA results were compared. The char yields (CY^{cal}) of TPU composites are calculated according to Eqs. (7) and (8)

$$CY^{cal} = CY_{TPU} \times f_{w,TPU} + CY_{CAPP} \times f_{w,CAPP} \quad (7)$$

$$CY^{cal} = CY_{TPU} \times f_{w,TPU} + CY_{CAPP} \times f_{w,CAPP} + CY_{MSCF} \times f_{w,MSCF} \quad (8)$$

where CY_{TPU}, CY_{CAPP}, and CY_{MSCF} respectively denote the residual yields of TPU, CAPP, and MSCF at 700 °C, and $f_{w,TPU}$, $f_{w,CAPP}$, and $f_{w,MSCF}$ refer to the weight fractions of TPU, CAPP, and MSCF in TPU composites, respectively.

The calculated values of thermo-gravimetric (TG) results are plotted in Figs. 4(b) and 4(d). Based on the above calculations,

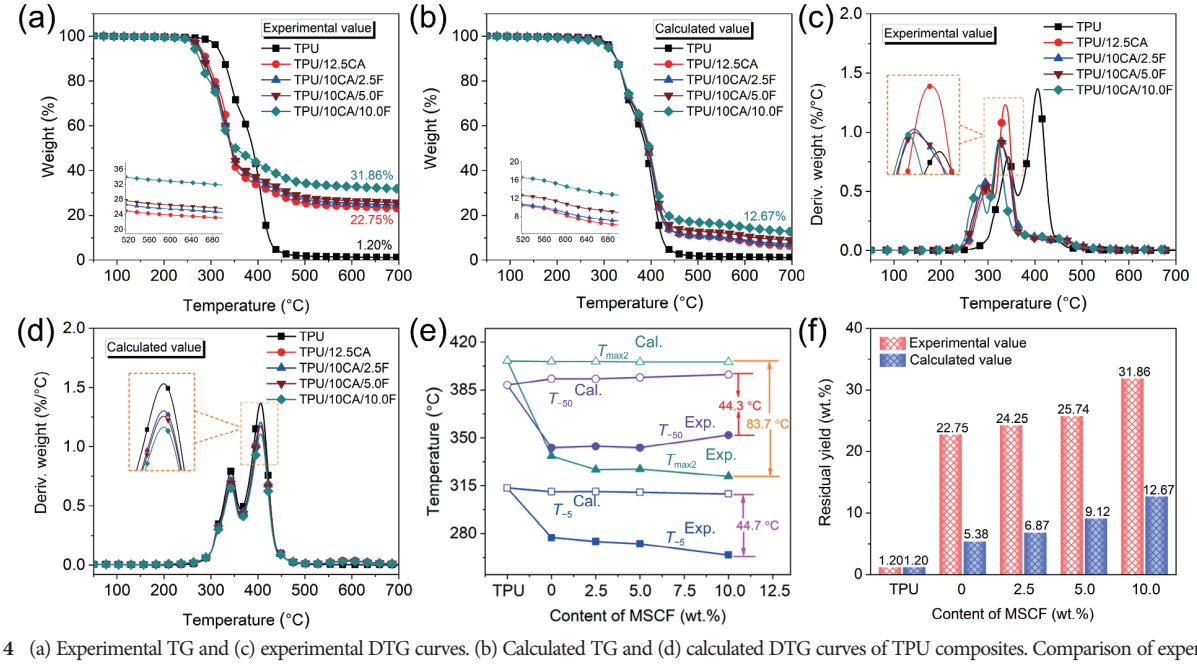

Figure 4 (a) Experimental TG and (c) experimental DTG curves. (b) Calculated TG and (d) calculated DTG curves of TPU composites. Comparison of experimental and calculated values of (e) T_{-5}, T_{-50}, and T_{max2}, and (f) residual yield.

different critical temperatures and residue yields are also compared in Figs. 4(e) and 4(f), respectively. The decomposition process of the experimental results and calculations are consistent. It is clearly found that T_{-5}, T_{-50}, and T_{max2} become lower in experimental results, whereas the char residues of the TPU composites in the experimental results are higher than those of the corresponding calculated results. Extraordinarily, TPU/10CA/10.0F exhibits the highest experimental char residues (31.86 wt.%) among all the TPU samples, which is 2.51 times higher than that of its calculated results. These phenomena affirm the synergistically catalytic charring between CAPP and MSCF.

3.4 Combustion behavior evaluation of TPU/CAPP/MSCF composites

Cone calorimeter is an instrument to evaluate combustion behavior of materials based on the principle of oxygen consumption [56, 57]. The cone calorimeter data of TPU composites at a heat flux of 35 kW/m^2 are presented in Fig. 6 and Table S2 in the ESM. It can be clearly found that the time to ignition (TTI) of all TPU composites are lower than that of pure TPU, which is consistent with the TGA results. As shown in Figs. 5(a) and 5(b), TPU shows high values of peak of heat release rate (PHRR) (870.1 kW/m^2) and total heat release (THR) (68.9 MJ/m^2) due to its inherent flammability. After the introduction of CAPP, the PHRR and THR of TPU/12.5CAPP are dramatically decreased by 75.9% and 69.1%, respectively. Furthermore, the TPU sample incorporated with 10.0 wt.% CAPP and 2.5 wt.% MSCF exhibits 77.8% and 58.6% reduction in PHRR and THR, respectively. The effect of inhibiting heat is more significant by using the same loading of MSCF to replace CAPP, indicating that MSCF and CAPP have a synergistic effect. However, more MSCF addition cannot lead to lower PHRR and THR. This phenomenon reveals the superior synergism between lower MSCF content and CAPP.

Smoke and toxic fumes are one of the most important factors affecting personnel escape and rescue when a fire happens. Therefore, it is quite necessary to detect smoke emission during the combustion. The peak of smoke production rate (PSPR) and total smoke release (TSR) data of TPU and its composites are summarized in Figs. 5(c) and 5(d), and Table S2 in the ESM. Pure TPU exhibits 0.1917 m^2/s of PSPR and 2,424.0 m^2/m^2 of TSR, respectively. In contrast to those of pure TPU, the PSPR and the TSR of TPU/12.5CA decline by 34.9% and 58.1%, respectively. However, there are slight increases in values of PSPR and TSR of TPU/10CA/F composites in comparison with those of TPU/12.5CA, meaning that the THR, SPR, and TSR of TPU composites filled with MSCF and CAPP are higher than those of TPU/12.5CA within 60 s of ignition. Overall, the introduction of MSCF into TPU/CAPP composites is beneficial to further reducing the HRR value, whereas the MSCF has little positive feedback on the THR, PSPR, and TSR. As recorded in Table S2 in the ESM, pure TPU exhibits little char residues left (4.72 wt.%). After the addition of CAPP, the remaining char residue increases to 56.78 wt.%. Unfortunately, the content of char residues of TPU composites decreases with the incorporation of MSCF and CAPP. These results can be attributed to the explanations that the addition of MSCF increases the strength of the char residues, which makes the char residue less likely to expand and foam, and leads to cracks of their char residues, causing the heat permeation and pyrolysis products release.

The flammability of TPU was also evaluated by LOI and UL-94 tests. The corresponding combustible data are listed in Table S2 in the ESM. Pure TPU shows only 21.7% of LOI. After the introduction of CAPP, TPU/12.5CA exhibits substantial improvement of LOI (26.2%). Then, the addition of MSCF and CAPP can make the value of LOI exceed 27%. Especially, the TPU/10CA/5.0F shows the highest LOI value (27.5%). In terms of vertical combustion test, pure TPU is endowed with no rating (NR) because of its inflammability, whereas the 12.5 wt.% CAPP renders TPU UL-94 V-1 rating. When 2.5 wt.% CAPP is replaced by the same loading level of MSCF, the TPU/10CA/2.5F achieves the UL-94 V-0 rating, demonstrating synergistic effect between MSCF and CAPP. With the increasing concentration of MSCF, the TPU/10CA/5.0F and the TPU/10CA/10.0F only reach the UL-94 V-2 rating. This phenomenon reveals that the excessive addition of MSCF will adversely affect the flame retardant properties of the TPU composites.

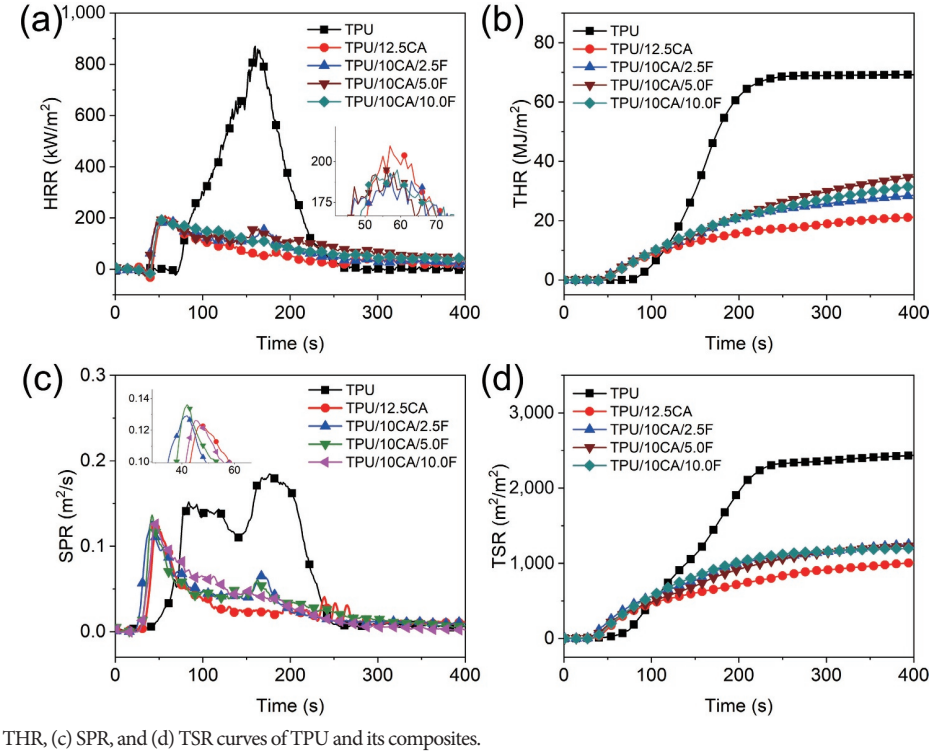

Figure 5 (a) HRR, (b) THR, (c) SPR, and (d) TSR curves of TPU and its composites.

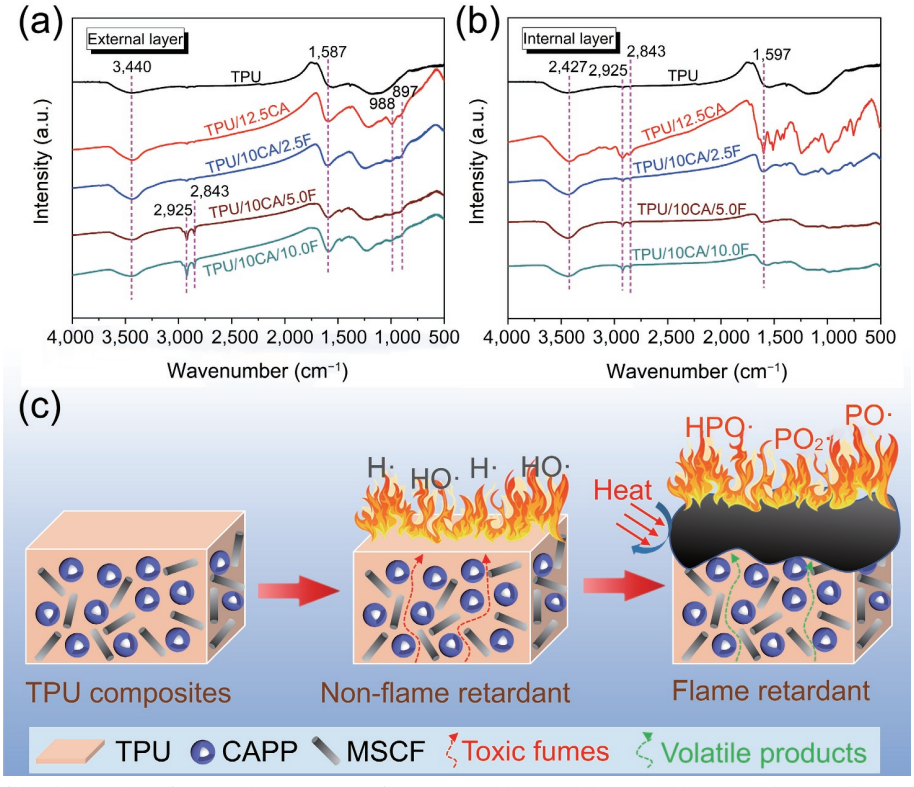

Figure 6 FTIR spectra of the char residues of TPU and its composites for (a) external layer and (b) internal layer; (c) schematic illustration for the flame retardant mechanism of TPU/CAPP/MSCF composites.

The digital photos of TPU composites after cone calorimeter test are presented in Fig. S2 in the ESM. From the top view (Fig. S2(a) in the ESM), surface pores of the char residue of TPU composites can be clearly observed. The char residues of pure TPU shows an incomplete structure with numerous cracks and voids, demonstrating its weak ability to suppress heat and toxic fumes. Upon the loading of 12.5 wt.% CAPP, the char residue of TPU/12.5CA becomes continuous. After the introduction of CAPP and MSC, the superficial char residues of TPU/CAPP/MSCF composites are robust with some micro-cracks, which weakens the ability of char residue to inhibit heat and smoke. The side view (Fig. S2(b) in the ESM) is helpful to observe the expansion of the char residues of TPU composites. Due to the existence of complete carbon, acid, and gas sources, the expansion height of char residues of the TPU/12.5CA reaches 3.8 cm. When 2.5 wt.% MSCF replaces the same loading of CAPP, the expansion height of char residues of the TPU/10CA/2.5F increases to 4.5 cm. This is due to the synergistic effect between CAPP and MSCF leading to generation of more incombustible gases. However, with increasing the mass ratio of MSCF to CAPP, the swelling height of the char residue of the TPU/CAPP/MSCF composites declines. The high loading of SCF makes the char layer difficult to expand. Furthermore, the production of large amounts of gas may lead to the ablation of the char layer underneath, resulting in the reduction of char residues of TPU composites.

SEM and LRS measurements can further reveal the microscopic morphology and structure of the char layers of TPU composites. Both external and internal layers of the expansive char residues of TPU composites are analyzed. Figure S3 in the ESM shows the external char residues of TPU composites. It is noted that char residue of pure TPU exhibits a loose and broken structure with numerous cavities (Figs. S3(a1) and S3(a2) in the ESM). After the introduction of CAPP, the surface of char residue of the TPU/12.5CA composite becomes continuous and compact (Figs. S3(b1) and S3(b2) in the ESM). With combination of MSCF and CAPP, incompletely degraded MSCF appears on the surface of the residual char of the TPU/CAPP/MSCF composites. It is worth noting that part of MSCF penetrates through the surface of the char residue of the TPU/CAPP/MSCF composites, leading to the discontinuous surface morphology (Figs. S3(c)–S3(e) in the ESM). LRS technique is performed to assess the degree of graphitization for char residues of TPU composites. As displayed in Fig. S3(f) in the ESM, LRS of external char residues of all TPU composites are fitted into two characteristic bands located at approximately 1,360 and 1,580 cm^{-1}, which correspond to D band and G band, and the integral area ratio of D to G band (A_D/A_G) is used to measure the graphitization degree of the char residue [58, 59]. Generally, the lower value of A_D/A_G means higher degree of graphitization. The A_D/A_G value of char residue of pure TPU is 2.71, whereas char residue of the TPU/12.5CA shows lower A_D/A_G value (2.49). After the incorporation of MSCF, the A_D/A_G values of char residues of TPU/CAPP/MSCF samples are higher than that of TPU/12.5CA. This can be due to the interpretations that the continuity of char residues of TPU/CAPP/MSCF composites is interrupted by the high loading of MSCF.

The SEM and LRS results of internal char residues for TPU and its composites are displayed in Fig. S4 in the ESM. Similar to the external char residue, internal char residue of pure TPU exhibits a porous structure (Fig. S4(a) in the ESM). With the addition of CAPP, the char residue of the TPU/12.5CA is more coherent and compact (Fig. S4(b) in the ESM). As plotted in Figs. S4(c)–S4(e) in the ESM, the surface of residual char of the TPU/CAPP/MSCF is relatively smooth with several cylindrical SCFs embedded and some voids observed. In comparison with external char residues of the TPU/CAPP and the TPU/CAPP/MSCF composites, their internal char residues present more continuous and impact profile. However, some cracks occur in the internal char residues of the TPU/CAPP/MSCF composites. These cracks provide the pathway for heat and smoke, which can explain why the relatively high values of THR, PSPR, and TSR for the TPU/CAPP/MSCF composites, as compared to those of the TPU/CAPP composite. Raman spectra of the internal char residues for all the TPU

samples are plotted in Fig. S4(f) in the ESM. The A_D/A_G values of char residues of TPU samples can be listed in a sequence of TPU/12.5CA (2.42) < TPU/10CA/10.0F (2.48) < TPU/10CA/2.5F (2.51) < TPU/10CA/5.0F (2.53) < TPU (2.71), suggesting that the TPU/12.5CA has the highest graphitization degree. It is noted that the microstructure of char residues of TPU and its composites is not well agreement with their Raman results, indicating the existence of multiple flame retardant mechanisms for TPU/CAPP/MSCF composites. According to the analysis aforementioned, the high quality of internal char residues instead of external char residues is principally responsible for the improved flame retardancy and smoke suppression.

FTIR technique is employed to dissect the chemical structure of the char residues for TPU and its composites, and the related spectra are depicted in Figs. 6(a) and 6(b). In the case of pure TPU, the intense band at 3,440 cm^{-1} is ascribed to hydroxyl group, and 1,587 cm^{-1} is attributed to aromatic compounds [45]. The char residue of the TPU/12.5CA presents two absorption bands at 988 (P–O–C stretching vibration) and 897 cm^{-1} (P–O stretching vibration), which are residual phosphorus-containing components after the decomposition of APP [60–62]. As the loading of MSCF reaches 5 wt.% or 10 wt.%, the new absorption bands at 2,843 and 2,925 cm^{-1} ascribed to the stretching vibration of CH_2 group become more pronounced [19, 63], indicating the promotive cross-linked ability of MSCF. It is noted that there is not an obvious band assigned to CAB shell after combustion, probably due to the complete evolution of CAB shell into char residues.

According to the analysis aforementioned, the possible flame retardant mechanism for TPU composites is presented in Fig. 6(c). The CAPP can work in both condensed and gas phases while MSCF mainly plays a role in the condensed phase. The CAB shell on the surface of APP which serves as a char source can promote the formation of an expanded char layer. In addition, CAPP can be decomposed into phosphoric acid and inert gas, which plays an important role in catalytic crosslinking and foaming expansion of char layer. Moreover, phosphorus-containing free radicals, including PO·, PO_2·, and HPO·, derived from APP can effectively capture the H· and HO· in the flame region. Incorporating a low loading of MSCF can endow TPU composites with the denser char residues. In general, the synergistic effect between CAPP and MSCF can effectively inhibit heat release and smoke generation.

3.5 EMI shielding evaluation of TPU/CAPP/MSCF-SW composites

The EMI shielding properties for multi-hierarchical flexible TPU composites with a thickness of around 1.00 mm (0.50 mm of TPU plate and 24.48 ± 1.19 μm of MXene film) at the frequency of X-band (8.2–12.4 GHz) and K-band (18.2–26.5 GHz) were investigated, as shown in Fig. 7. Total EMI SE curves of the TPU composites are plotted in Figs. 7(a) and 7(b). The obtained EMI SE results are similar in X band and K band. The SE_T of pure TPU is near to zero, indicating its inability to electromagnetic shielding. It is evident that SE_T value of the TPU-SW with MXene film has greatly improved due to the high electrical conductivity of $Ti_3C_2T_x$. Nevertheless, the TPU/12.5CA-SW shows higher SE_T than the TPU-SW, benefiting from the scattering effect of CAPP on electromagnetic waves. Then, the EMI SE values of the TPU composites gradually increase with increment of MSCF content from 2.5 wt.% to 10.0 wt.%. The outstanding EMI SE implies the advantage of shielding electromagnetic waves by MSCF. Specially, the SE_T of TPU/CAPP/MSCF-SW fluctuates with the different frequencies which is probably due to the sampling location or impedance mismatch. The MSCF is uniformly dispersed in the TPU matrix during the melt blending process. Therefore, satisfactory loading of MSCF can easily promote the formation of a conductive network.

Average SE_T, SE_R, and SE_A values for TPU composites at the frequency of X band and K band are shown in Figs. 7(c) and 7(d), respectively. It can be clearly found that the EMI SE values of the TPU composites are higher in the X band than their corresponding values in the K band. For example, the SE_T values of the TPU/10CA/10.0F-SW in the X band and K band reach 43.8 and 32.0 dB, respectively. The increasing trend of the SE_A shows a good agreement with that of the SE_T in all TPU samples. Moreover, the SE_A values of TPU composites are greatly higher than their corresponding SE_R values, indicating the strong ability of absorbing electromagnetic waves [64].

In order to reveal the electromagnetic shielding mechanism of

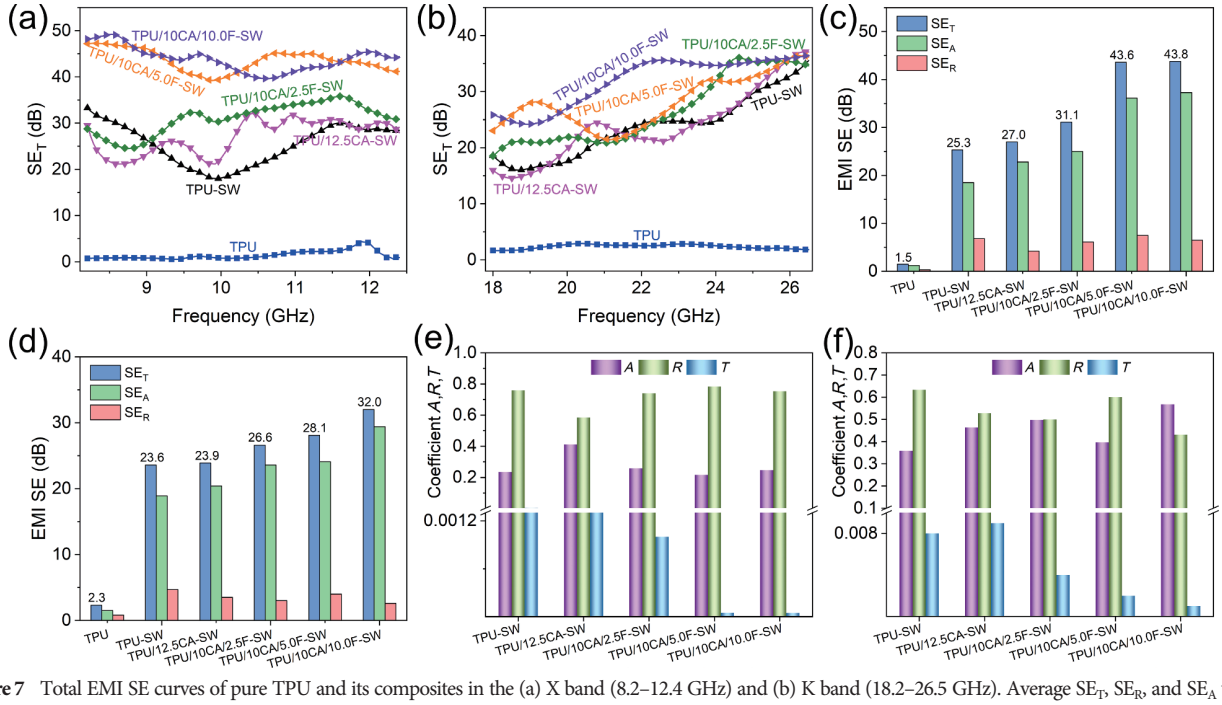

Figure 7 Total EMI SE curves of pure TPU and its composites in the (a) X band (8.2–12.4 GHz) and (b) K band (18.2–26.5 GHz). Average SE_T, SE_R, and SE_A values of pure TPU and its composites in the (c) X band and (d) K band. Average *A*, *R*, and *T* coefficient of TPU composites in the (e) X band and (f) K band.

multi-hierarchical flexible TPU composites. The average *A*, *R*, and *T* coefficient of the obtained TPU samples were also analyzed, as shown in Figs. 7(e) and 7(f). In the X band, compared to the *R* coefficient of TPU-SW, the *R* coefficient of TPU/12.5CA-SW decreases and then increases after the loading of SCF. However, the variation tendency of the *A* coefficient is the opposite. Generally, *R* coefficient of TPU samples is higher than their corresponding *A* coefficient (Fig. 7(e)). In this case, reflection can be regarded as the dominant shielding mechanism [65]. Especially, the *R* coefficient of the TPU/10CA/5.0F-SW reaches approximately 0.60. This is due to the high electrical conductivity and multiple layer structure of MXene film. The electromagnetic wave is reflected multiple times within the MXene film and then attenuated in this process. In brief, high reflection prolongs the transmission path of electromagnetic waves, which is equivalent to increasing the thickness of the material. Similarly, TPU composites show the same patterns in K band (Fig. 7(f)) as those in X band.

To vividly illustrate the EMI shielding mechanism of as-prepared multi-hierarchical flexible TPU composites, the diagram for possible mechanism is proposed in Fig. 8. As the incident electromagnetic waves radiate into the surface of the TPU composites, impedance mismatch occurs at different phase interfaces. As a result, part of the incident waves is reflected on the surface without entering the interior of the TPU host. Then, the transmitted electromagnetic waves propagate in TPU plate. CAPP dispersed in the TPU composites has a scattering effect on electromagnetic waves while MSCF shows a radiation effect [19]. When the loading of MSCF increases, integrated conductive networks are gradually formed. Therefore, after passing through the first layer of TPU samples, the incident electromagnetic waves are partially attenuated. Subsequently, the incident waves propagate from the TPU layer to the MXene film. The regular hierarchical structure of MXene films can cause multiple reflections, scattering, and absorption, which lengthens the path the propagation of electromagnetic waves and attenuates the waves substantially. The propagation of electromagnetic waves drives the movement of the charge carriers, thereby dissipating them in the form of thermal energy [34]. In addition, the distribution of free carriers easily leads to polarization at the TPU/MXene interface, which is conducive to further absorption of electromagnetic waves. Finally, the remaining waves permeate into another TPU layer. Attenuation of electromagnetic waves similar to the above process occurs. Only a small part of the electromagnetic waves can escape through the TPU matrix, indicating that the TPU/CAPP/MSCF composites have excellent EMI shielding performance.

3.6 Performance comparison

The comparison of EMI shielding effect between our work and previously reported TPU-based polymeric composites is illustrated in Table 2. Conductive fillers, including carbon nanotubes, graphene, carbon fiber, and titanium carbide, are well arranged into TPU matrix. And the TPU composites are usually fabricated by solution mixing, melt blending, or constructing porous structure or hierarchical structure and so on. The TPU/10CA/10.0F-SW with a thickness of 1.0 mm shows prominent EMI SE (43.8 dB) among all the samples. Moreover, compared with only a single electromagnetic shielding performance, integrating both flame retardant and electromagnetic shielding properties can greatly broaden the application field of TPU material. In conclusion, the multi-hierarchical flexible composites prepared in our work are superior to the reported previous work.

4 Conclusions

In this work, a series of novel multi-hierarchical flexible TPU composites were fabricated by constructing TPU plates loaded with CAPP and MSCF as surface layer while MXene film as interlayer. The obtained results indicated that the TPU/CAPP/MSCF composites presented outstanding interface compatibility and high thermal stability by comparing theoretical calculations and experimental results. With the incorporation of 10.0 wt.% CAPP and 2.5 wt.% MSCF, the TPU composites obtained UL-94 V-0 rating and the decreased PHRR (77.8% reduction) compared to pure TPU. However, in comparation with those of the TPU/12.5CA, the THR, PSPR, and TSR of TPU/CAPP/SCF had a slightly increase due to the cracked char residues. Furthermore, our work also shows superiority in electromagnetic shielding performance compared with previously reported work. The average EMI SE values of TPU composites filled with 10 wt.% CAPP and 10 wt.% MSCF were 43.8 and 32.0 dB in X band and K band, respectively. Generally, in order to manufacture multi-hierarchical flexible TPU composites integrated with prominent EMI shielding and flame retardant properties, it is necessary to establish a balance between the flame retardants and the conductive fillers.

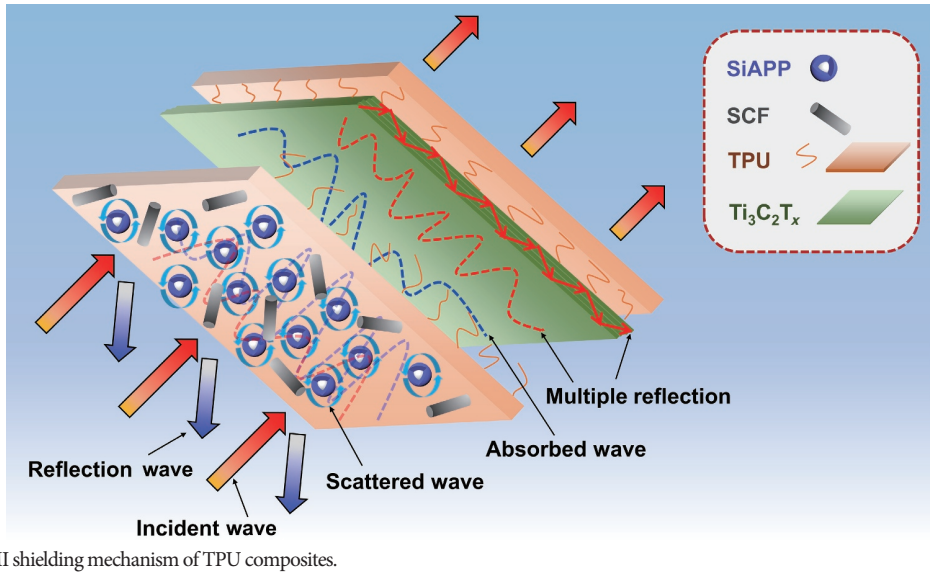

Figure 8 Proposed EMI shielding mechanism of TPU composites.

Table 2 Comparison of electromagnetic shielding effectiveness of TPU-based polymeric composites

Sample No.	Conductive filler content	Thickness	Structure	EMI SE	Flame retardancy	References
PANI/FMWCNT/TPU	PANI/8 wt.% FMWCNT	1.0 mm	Solution mixing	31.35 dB	No	[18]
PUG	20 wt.% graphene	6.5 mm	Porous structure	23-24 dB	No	[66]
$Ti_3C_2T_x$ MXene/CFf/TPU	$Ti_3C_2T_x$/CFf weight ratio = 1.06%	0.5 mm	Sandwich	40.4 dB	No	[24]
TPU/CB-PPy/CNT	8 wt.% CB-PPy/CNT	2.0 mm	Melt blending	39.52 dB	No	[67]
TPU/CNTs	10 wt.% CNT	1.2 mm	Solution mixing	42.5 dB	No	[68]
EG–TPU–PVDF	EG/PVDF mass ratio = 6/10	0.74 mm	Multilayer	21.4 dB	No	[69]
TPU/rGO-Salen-Ni	8 wt.% rGO-Salen-Ni	0.5 mm	Solution mixing	11.5 dB	Yes	[42]
TPU/IFR/CNT	IFR/CNT mass ratio = 10/1	1.6 mm	Melt blending	20.0 dB	Yes	[70]
TPU/PBS/IFRs/MWCNTs	PBS/MWCNTs mass ratio = 1/3	2.4 mm	Segregated structure	45 dB	Yes	[71]
PBS-CNT/TPU-IFR-CNT	7 wt.% CNTs	1.7 mm	Multilayer	30 dB	Yes	[33]
TPU/10CA/10.0F-SW	10 wt.% MSCF	1.0 mm	Multi-hierarchical	43.8 dB	Yes	This work

Acknowledgements

This work was financially supported by the National Natural Science Foundation of China (Nos. 52173070 and 51803031). The authors thank Dr. Jianhang Lin, Dr. Qingming Huang and Dr. Na Ai of Fujian College Association Instrumental Analysis Center for assisting analysis of SEM images, XRD patterns and Raman spectra, respectively.

Electronic Supplementary Material: Supplementary material (TGA data, cone calorimeter data, XRD patterns, FTIR spectra, XPS survey spectra, TG curves, and SEM images) is available in the online version of this article at https://doi.org/10.1007/s12274-022-4883-6.

References

[1] Gao, C. Q.; Shi, Y. Q.; Chen, Y. J.; Zhu, S. C.; Feng, Y. Z.; Lv, Y. C.; Yang, F. Q.; Liu, M. H.; Shui, W. Constructing segregated polystyrene composites for excellent fire resistance and electromagnetic wave shielding. *J. Colloid Interface Sci.* **2022**, *606*, 1193–1204.

[2] Sun, Z. P.; Chen, J. L.; Jia, X. C.; Wang, G. Q.; Shen, B.; Zheng, W. G. Humidification of high-performance and multifunctional polyimide/carbon nanotube composite foams for enhanced electromagnetic shielding. *Mater. Today Phys.* **2021**, *21*, 100521.

[3] Ma, Z. L.; Xiang, X. L.; Shao, L.; Zhang, Y. L.; Gu, J. W. Multifunctional wearable silver nanowire decorated leather nanocomposites for joule heating, electromagnetic interference shielding and piezoresistive sensing. *Angew. Chem., Int. Ed.* **2022**, *61*, e202200705.

[4] Shen, B.; Zhai, W. T.; Zheng, W. G. Ultrathin flexible graphene film: An excellent thermal conducting material with efficient EMI shielding. *Adv. Funct. Mater.* **2014**, *24*, 4542–4548.

[5] Zhang, Y. L.; Kong, J.; Gu, J. W. New generation electromagnetic materials: Harvesting instead of dissipation solo. *Sci. Bull.* **2022**, *67*, 1413–1415.

[6] Pan, M. Z.; Mei, C. T.; Du, J.; Li, G. C. Synergistic effect of Nano silicon dioxide and ammonium polyphosphate on flame retardancy of wood fiber-polyethylene composites. *Compos. Part A:Appl. Sci. Manuf.* **2014**, *66*, 128–134.

[7] Savas, L. A.; Deniz, T. K.; Tayfun, U.; Dogan, M. Effect of microcapsulated red phosphorus on flame retardant, thermal and mechanical properties of thermoplastic polyurethane composites filled with huntite&hydromagnesite mineral. *Polym. Degrad. Stabil.* **2017**, *135*, 121–129.

[8] Wilke, A.; Langfeld, K.; Ulmer, B.; Andrievici, V.; Hörold, A.; Limbach, P.; Bastian, M.; Schartel, B. Halogen-free multicomponent flame retardant thermoplastic styrene-ethylene-butylene-styrene elastomers based on ammonium polyphosphate-expandable graphite synergy. *Ind. Eng. Chem. Res.* **2017**, *56*, 8251–8263.

[9] Sut, A.; Metzsch-Zilligen, E.; Großhauser, M.; Pfaendner, R.; Schartel, B. Synergy between melamine cyanurate, melamine polyphosphate and aluminum diethylphosphinate in flame retarded thermoplastic polyurethane. *Polym. Test.* **2019**, *74*, 196–204.

[10] Zhu, M.; Zhang, Y.; Sheng, H. B.; Wang, B. B.; Hu, Y. Effect carbon black microencapsulated ammonium polyphosphate on the flame retardancy and mechanical properties of polyurethane composites. *Polym. Plast. Technol. Mater.* **2020**, *59*, 83–94.

[11] Gao, W. Y.; Qian, X. D.; Wang, S. J. Preparation of hybrid silicon materials microcapsulated ammonium polyphosphate and its application in thermoplastic polyurethane. *J. Appl. Polym. Sci.* **2018**, *135*, 45742.

[12] Bahri, Z. E.; Taverdet, J. L. Preparation and optimization of 2,4-D loaded cellulose derivatives microspheres by solvent evaporation technique. *J. Appl. Polym. Sci.* **2007**, *103*, 2742–2751.

[13] Wang, B. B.; Tang, Q. B.; Hong, N. N.; Song, L.; Wang, L.; Shi, Y. Q.; Hu, Y. Effect of cellulose acetate butyrate microencapsulated ammonium polyphosphate on the flame retardancy, mechanical, electrical, and thermal properties of intumescent flame-retardant ethylene-vinyl acetate copolymer/microencapsulated ammonium polyphosphate/polyamide-6 blends. *ACS Appl. Mater. Interfaces* **2011**, *3*, 3754–3761.

[14] Kuzhir, P.; Paddubskaya, A.; Bychanok, D.; Liubimau, A.; Ortona, A.; Fierro, V.; Celzard, A. 3D-printed, carbon-based, lossy photonic crystals: Is high electrical conductivity the must? *Carbon* **2021**, *171*, 484–492.

[15] Letellier, M.; Macutkevic, J.; Kuzhir, P.; Banys, J.; Fierro, V.; Celzard, A. Electromagnetic properties of model vitreous carbon foams. *Carbon* **2017**, *122*, 217–227.

[16] Kuzhir, P. P.; Paddubskaya, A. G.; Volynets, N. I.; Batrakov, K. G.; Kaplas, T.; Lamberti, P.; Kotsilkova, R.; Lambin, P. Main principles of passive devices based on graphene and carbon films in microwave-THz frequency range. *J. Nanophotonics.* **2017**, *11*, 032504.

[17] Lecocq, H.; Garois, N.; Lhost, O.; Girard, P. F.; Cassagnau, P.; Serghei, A. Polypropylene/carbon nanotubes composite materials with enhanced electromagnetic interference shielding performance: Properties and modeling. *Compos. Part B:Eng.* **2020**, *189*, 107866.

[18] Sobha, A. P.; Sreekala, P. S.; Narayanankutty, S. K. Electrical, thermal, mechanical and electromagnetic interference shielding properties of PANI/FMWCNT/TPU composites. *Prog. Org. Coat.* **2017**, *113*, 168–174.

[19] Duan, N. M.; Shi, Z. Y.; Wang, J. L.; Wang, G. L.; Zhang, X. Z. Strong and flexible carbon fiber fabric reinforced thermoplastic polyurethane composites for high-performance EMI shielding applications. *Macromol. Mater. Eng.* **2020**, *305*, 1900829.

[20] Lu, J. Y.; Zhang, Y.; Tao, Y. J.; Wang, B. B.; Cheng, W. H.; Jie, G. X.; Song, L.; Hu, Y. Self-healable castor oil-based waterborne polyurethane/MXene film with outstanding electromagnetic interference shielding effectiveness and excellent shape memory performance. *J. Colloid Interface Sci.* **2021**, *588*, 164–174.

[21] Verma, M.; Chauhan, S. S.; Dhawan, S. K.; Choudhary, V. Graphene

nanoplatelets/carbon nanotubes/polyurethane composites as efficient shield against electromagnetic polluting radiations. *Compos. Part B:Eng.* **2017**, *120*, 118–127.

[22] Batrakov, K.; Kuzhir, P.; Maksimenko, S.; Volynets, N.; Voronovich, S.; Paddubskaya, A.; Valusis, G.; Kaplas, T.; Svirko, Y.; Lambin, P. Enhanced microwave-to-terahertz absorption in graphene. *Appl. Phys. Lett.* **2016**, *108*, 123101.

[23] Yang, W. X.; Zhao, Z. D.; Wu, K.; Huang, R.; Liu, T. Y.; Jiang, H.; Chen, F.; Fu, Q. Ultrathin flexible reduced graphene oxide/cellulose nanofiber composite films with strongly anisotropic thermal conductivity and efficient electromagnetic interference shielding. *J. Mater. Chem. C* **2017**, *5*, 3748–3756.

[24] Duan, N. M.; Shi, Z. Y.; Wang, Z. H.; Zou, B.; Zhang, C. P.; Wang, J. L.; Xi, J. R.; Zhang, X. S.; Zhang, X. Z.; Wang, G. L. Mechanically robust $Ti_3C_2T_x$ MXene/carbon fiber fabric/thermoplastic polyurethane composite for efficient electromagnetic interference shielding applications. *Mater. Design* **2022**, *214*, 110382.

[25] Yin, X. C.; Wang, L.; Li, S.; He, G. J.; Yang, Z. T.; Feng, Y. H.; Qu, J. P. Preparation and characterization of carbon fiber/polylactic acid/thermoplastic polyurethane (CF/PLA/TPU) composites prepared by a vane mixer. *J. Polym. Eng.* **2017**, *37*, 355–364.

[26] Lin, S. C.; Ma, C. C. M.; Hsiao, S. T.; Wang, Y. S.; Yang, C. Y.; Liao, W. H.; Li, S. M.; Wang, J. A.; Cheng, T. Y.; Lin, C. W. et al. Electromagnetic interference shielding performance of waterborne polyurethane composites filled with silver nanoparticles deposited on functionalized graphene. *Appl. Surf. Sci.* **2016**, *385*, 436–444.

[27] Li, J. W.; Ding, Y. Q.; Yu, N.; Gao, Q.; Fan, X.; Wei, X.; Zhang, G. C.; Ma, Z. L.; He, X. H. Lightweight and stiff carbon foams derived from rigid thermosetting polyimide foam with superior electromagnetic interference shielding performance. *Carbon* **2020**, *158*, 45–54.

[28] Ji, X. Y.; Chen, D. Y.; Shen, J. B.; Guo, S. Y. Flexible and flame-retarding thermoplastic polyurethane-based electromagnetic interference shielding composites. *Chem. Eng. J.* **2019**, *370*, 1341–1349.

[29] Sun, Z. P.; Shen, B.; Li, Y.; Chen, J. L.; Zheng, W. G. High-performance porous carbon foams via catalytic pyrolysis of modified isocyanate-based polyimide foams for electromagnetic shielding. *Nano Res.* **2022**, *15*, 6851–6859.

[30] Zhang, Y.; Xu, M. K.; Wang, Z. G.; Zhao, T. Y.; Liu, L. X.; Zhang, H. B.; Yu, Z. Z. Strong and conductive reduced graphene oxide-MXene porous films for efficient electromagnetic interference shielding. *Nano Res.* **2022**, *15*, 4916–4924.

[31] Feng, D.; Wang, Q. Q.; Xu, D. W.; Liu, P. J. Microwave assisted sinter molding of polyetherimide/carbon nanotubes composites with segregated structure for high-performance EMI shielding applications. *Compos. Sci. Technol.* **2019**, *182*, 107753.

[32] Gao, Q. S.; Pan, Y. M.; Zheng, G. Q.; Liu, C. T.; Shen, C. Y.; Liu, X. H. Flexible multilayered MXene/thermoplastic polyurethane films with excellent electromagnetic interference shielding, thermal conductivity, and management performances. *Adv. Compos. Hybrid Mater.* **2021**, *4*, 274–285.

[33] He, L.; Shi, Y. D.; Wang, Q. W.; Chen, D. Y.; Shen, J. B.; Guo, S. Y. Strategy for constructing electromagnetic interference shielding and flame retarding synergistic network in poly(butylene succinate) and thermoplastic polyurethane multilayered composites. *Compos. Sci. Technol.* **2020**, *199*, 108324.

[34] Zhang, Y. L.; Ruan, K. P.; Gu, J. W. Flexible sandwich-structured electromagnetic interference shielding nanocomposite films with excellent thermal conductivities. *Small* **2021**, *17*, 2101951.

[35] Liu, C.; Wu, W.; Shi, Y. Q.; Yang, F. Q.; Liu, M. H.; Chen, Z. X.; Yu, B.; Feng, Y. Z. Creating MXene/reduced graphene oxide hybrid towards highly fire safe thermoplastic polyurethane nanocomposites. *Compos. Part B:Eng.* **2020**, *203*, 108486.

[36] Liu, C.; Yao, A. S.; Chen, K. X.; Shi, Y. Q.; Feng, Y. Z.; Zhang, P.; Yang, F. Q.; Liu, M. H.; Chen, Z. X. MXene based core–shell flame retardant towards reducing fire hazards of thermoplastic polyurethane. *Compos. Part B: Eng.* **2021**, *226*, 109363.

[37] Zhang, Y. L.; Ma, Z. L.; Ruan, K. P.; Gu, J. W. Multifunctional $Ti_3C_2T_x$-(Fe_3O_4/polyimide) composite films with Janus structure for outstanding electromagnetic interference shielding and superior visual thermal management. *Nano Res.* **2022**, *15*, 5601–5609.

[38] Zhang, Y. L.; Yan, Y.; Qiu, H.; Ma, Z. L.; Ruan, K. P.; Gu, J. W. A mini-review of MXene porous films: Preparation, mechanism and application. *J. Mater. Sci. Technol.* **2022**, *103*, 42–49.

[39] Jiao, C. Y.; Deng, Z. M.; Min, P.; Lai, J. J.; Gou, Q. Q.; Gao, R.; Yu, Z. Z.; Zhang, H. B. Photothermal healable, stretchable, and conductive MXene composite films for efficient electromagnetic interference shielding. *Carbon* **2022**, *198*, 179–187.

[40] Shi, Y. Q.; Liu, C.; Duan, Z. P.; Yu, B.; Liu, M. H.; Song, P. G. Interface engineering of MXene towards super-tough and strong polymer nanocomposites with high ductility and excellent fire safety. *Chem. Eng. J.* **2020**, *399*, 125829.

[41] Shi, Y. Q.; Liu, C.; Liu, L.; Fu, L. B.; Yu, B.; Lv, Y. C.; Yang, F. Q.; Song, P. A. Strengthening, toughing and thermally stable ultra-thin MXene nanosheets/polypropylene nanocomposites via nanoconfinement. *Chem. Eng. J.* **2019**, *378*, 122267.

[42] Wei, W. C.; Deng, C.; Huang, S. C.; Wei, Y. X.; Wang, Y. Z. Nickel-Schiff base decorated graphene for simultaneously enhancing the electroconductivity, fire resistance, and mechanical properties of a polyurethane elastomer. *J. Mater. Chem. A* **2018**, *6*, 8643–8654.

[43] Scheibe, B.; Tadyszak, K.; Jarek, M.; Michalak, N.; Kempiński, M.; Lewandowski, M.; Peplińska, B.; Chybczyńska, K. Study on the magnetic properties of differently functionalized multilayered $Ti_3C_2T_x$ MXenes and Ti-Al-C carbides. *Appl. Surf. Sci.* **2019**, *479*, 216–224.

[44] Shah, S. A.; Habib, T.; Gao, H.; Gao, P.; Sun, W.; Green, M. J.; Radovic, M. Template-free 3D titanium carbide ($Ti_3C_2T_x$) MXene particles crumpled by capillary forces. *Chem. Commun.* **2017**, *53*, 400–403.

[45] Liu, L. B.; Xu, Y.; Li, S.; Xu, M. J.; He, Y. T.; Shi, Z. X.; Li, B. A novel strategy for simultaneously improving the fire safety, water resistance and compatibility of thermoplastic polyurethane composites through the construction of biomimetic hydrophobic structure of intumescent flame retardant synergistic system. *Compos. Part B: Eng.* **2019**, *176*, 107218.

[46] Wei, W.; Huang, X. B.; Chen, K. Y.; Tao, Y. M.; Tang, X. Z. Fluorescent organic–inorganic hybrid polyphosphazene microspheres for the trace detection of nitroaromatic explosives. *RSC Adv.* **2012**, *2*, 3765–3771.

[47] Zhang, X. Q.; Xu, H. B.; Fan, X. Y. Grafting of amine-capped cross-linked polyphosphazenes onto carbon fiber surfaces: A novel coupling agent for fiber reinforced composites. *RSC Adv.* **2014**, *4*, 12198–12205.

[48] Tran, M. Q.; Ho, K. K. C.; Kalinka, G.; Shaffer, M. S. P.; Bismarck, A. Carbon fibre reinforced poly(vinylidene fluoride): Impact of matrix modification on fibre/polymer adhesion. *Compos. Sci. Technol.* **2008**, *68*, 1766–1776.

[49] Wu, Z. H.; Pittman, C. U. Jr; Gardner, S. D. Nitric acid oxidation of carbon fibers and the effects of subsequent treatment in refluxing aqueous NaOH. *Carbon* **1995**, *33*, 597–605.

[50] Biniak, S.; Szymański, G.; Siedlewski, J.; Świątkowski, A. The characterization of activated carbons with oxygen and nitrogen surface groups. *Carbon* **1997**, *35*, 1799–1810.

[51] Georgiou, P.; Walton, J.; Simitzis, J. Surface modification of pyrolyzed carbon fibres by cyclic voltammetry and their characterization with XPS and dye adsorption. *Electrochim. Acta* **2010**, *55*, 1207–1216.

[52] Crobu, M.; Rossi, A.; Mangolini, F.; Spencer, N. D. Chain-length-identification strategy in zinc polyphosphate glasses by means of XPS and ToF-SIMS. *Anal. Bioanal. Chem.* **2012**, *403*, 1415–1432.

[53] Chen, K. X.; Feng, Y. Z.; Shi, Y. Q.; Wang, H. R.; Fu, L. B.; Liu, M.; Lv, Y. C.; Yang, F. Q.; Yu, B.; Liu, M. H. et al. Flexible and fire safe sandwich structured composites with superior electromagnetic interference shielding properties. *Compos. Part A: Appl. Sci. Manuf.* **2022**, *160*, 107070.

[54] Chen, X. L.; Jiao, C. M.; Zhang, J. Microencapsulation of ammonium polyphosphate with hydroxyl silicone oil and its flame retardance in thermoplastic polyurethane. *J. Therm. Anal. Calorim.* **2011**, *104*, 1037–1043.

[55] Green, J. A review of phosphorus-containing flame retardants. *J. Fire Sci.* **1992**, *10*, 470–487.

[56] Liu, C.; Xu, K.; Shi, Y. Q.; Wang, J. W.; Ma, S. N.; Feng, Y. Z.; Lv, Y. C.; Yang, F. Q.; Liu, M. H.; Song, P. G. Fire-safe, mechanically strong and tough thermoplastic Polyurethane/MXene nanocomposites with exceptional smoke suppression. *Mater. Today Phys.* **2022**, *22*, 100607.

[57] Zhang, Y.; Jing, J.; Liu, T.; Xi, L. D.; Sai, T.; Ran, S. Y.; Fang, Z. P.; Huo, S. Q.; Song, P. G. A molecularly engineered bioderived polyphosphate for enhanced flame retardant, UV-blocking and mechanical properties of poly(lactic acid). *Chem. Eng. J.* **2021**, *411*, 128493.

[58] Yuan, Y.; Wang, W.; Shi, Y. Q.; Song, L.; Ma, C.; Hu, Y. The influence of highly dispersed Cu_2O-anchored MoS_2 hybrids on reducing smoke toxicity and fire hazards for rigid polyurethane foam. *J. Hazard. Mater.* **2020**, *382*, 121028.

[59] Wu, W.; Zhao, W. J.; Gong, X. J.; Sun, Q. J.; Cao, X. W.; Su, Y. J.; Yu, B.; Li, R. K. Y.; Vellaisamy, R. A. L. Surface decoration of Halloysite nanotubes with POSS for fire-safe thermoplastic polyurethane nanocomposites. *J. Mater. Sci. Technol.* **2022**, *101*, 107–117.

[60] Ni, J. X.; Chen, L. J.; Zhao, K. M.; Hu, Y.; Song, L. Preparation of gel-silica/ammonium polyphosphate core–shell flame retardant and properties of polyurethane composites. *Polym. Adv. Technol.* **2011**, *22*, 1824–1831.

[61] Ren, Y. L.; Zhang, Y.; Gu, Y. T.; Zeng, Q. Flame retardant polyacrylonitrile fabrics prepared by organic–inorganic hybrid silica coating via sol-gel technique. *Prog. Org. Coat.* **2017**, *112*, 225–233.

[62] Rajaei, M.; Wang, D. Y.; Bhattacharyya, D. Combined effects of ammonium polyphosphate and talc on the fire and mechanical properties of epoxy/glass fabric composites. *Compos. Part B: Eng.* **2017**, *113*, 381–390.

[63] Bian, R. J.; Lin, R. Z.; Wang, G. L.; Lu, G.; Zhi, W. Q.; Xiang, S. L.; Wang, T. W.; Clegg, P. S.; Cai, D. Y.; Huang, W. 3D assembly of Ti_3C_2-MXene directed by water/oil interfaces. *Nanoscale* **2018**, *10*, 3621–3625.

[64] Fan, Z. M.; Wang, D. L.; Yuan, Y.; Wang, Y. S.; Cheng, Z. J.; Liu, Y. Y.; Xie, Z. M. A lightweight and conductive MXene/graphene hybrid foam for superior electromagnetic interference shielding. *Chem. Eng. J.* **2020**, *381*, 122696.

[65] Peng, M. Y.; Qin, F. X. Clarification of basic concepts for electromagnetic interference shielding effectiveness. *J. Appl. Phys.* **2021**, *130*, 225108.

[66] Li, Y.; Shen, B.; Yi, D.; Zhang, L. H.; Zhai, W. T.; Wei, X. C.; Zheng, W. G. The influence of gradient and sandwich configurations on the electromagnetic interference shielding performance of multilayered thermoplastic polyurethane/graphene composite foams. *Compos. Sci. Technol.* **2017**, *138*, 209–216.

[67] Bertolini, M. C.; Ramoa, S. D. A. S.; Merlini, C.; Barra, G. M. O.; Soares, B. G.; Pegoretti, A. Hybrid composites based on thermoplastic polyurethane with a mixture of carbon nanotubes and carbon black modified with polypyrrole for electromagnetic shielding. *Front. Mater.* **2020**, *7*, 174.

[68] Shin, B.; Mondal, S.; Lee, M.; Kim, S.; Huh, Y. I.; Nah, C. Flexible thermoplastic polyurethane-carbon nanotube composites for electromagnetic interference shielding and thermal management. *Chem. Eng. J.* **2021**, *418*, 129282.

[69] Dong, W. Q.; He, L.; Chen, C. Q.; Kang, J.; Niu, H. M.; Zhang, J. B.; Li, J.; Li, K. S. Preparation and electromagnetic shielding performances of graphene/TPU-PVDF nanocomposites by high-energy ball milling. *J. Mater. Sci. Mater. Electron.* **2022**, *33*, 1817–1829.

[70] Ji, X. Y.; Chen, D. Y.; Wang, Q. W.; Shen, J. B.; Guo, S. Y. Synergistic effect of flame retardants and carbon nanotubes on flame retarding and electromagnetic shielding properties of thermoplastic polyurethane. *Compos. Sci. Technol.* **2018**, *163*, 49–55.

[71] Shi, Y. D.; He, L.; Chen, D. Y.; Wang, Q. W.; Shen, J. B.; Guo, S. Y. Simultaneously improved electromagnetic interference shielding and flame retarding properties of poly(butylene succinate)/thermoplastic polyurethane blends by constructing segregated flame retardants and multi-walled carbon nanotubes double network. *Compos. Part A: Appl. Sci. Manuf.* **2020**, *137*, 106037.